Computers and Electronics in Agriculture 152 (2018) 221–232

Contents lists available at ScienceDirect

Computers and Electronics in Agriculture

journal homepage: www.elsevier.com/locate/compag

Original papers

Asphyxia occurrence detection in sows during the farrowing phase by inter-birth interval evaluation

Cedric Okinda, Mingzhou Lu, Innocent Nyalala, Jiawei Li, Mingxia Shen*

College of Engineering, Laboratory of Modern Facility Agriculture Technology and Equipment Engineering of Jiangsu Province, Nanjing Agricultural University, Jiangsu 210031, PR China

ARTICLE INFO

Keywords:
Infrared depth image
Parametrized ellipse-fitting
Piglet mortality
Piglet vitality
Stillbirths

ABSTRACT

The occurrence of asphyxia in sows during parturition often results in stillbirths and low vitality piglets, thus significantly affecting pig production and animal welfare in terms of piglet mortality. The losses during farrowing can account to a significant loss in a litter, a whole litter or in extreme cases, the loss of the sow. The objective of this study was to develop an infrared depth image sensor-based monitoring system as a surveillance support system for stockmen during the farrowing phase of sows, in an effort to reduce piglet mortality associated with asphyxiation of piglets. Experiments were performed at Jurong Research farm of Nanjing Agricultural University, using a herd of 105 Meishan sows. Data was collected by monitoring the farrowing process of 15 sows housed in farrowing pens. The sows were monitored by video recording for labeling and depth images taken at 10 fpm for automatic system development. Data labeling was based on the timestamps of births of all the piglets in a litter and each piglet vitality score based on the number of times a piglet attempts to stand within the 1st minute after birth. Data labeling was performed 1 h before the start of parturition until 0.5 h after the end of parturition. The depth images were processed to segment the piglets, and a developed parametrized ellipse-fitting algorithm performed piglet detection by multi-ellipse fitting. Piglet count and count tracking were established by the number of fitted ellipses on the image-object shape. Each sequential increment in the piglet count was used to compute the inter-birth interval. The developed model attained a detection accuracy of 0.832 for no piglets and 0.801 for 14 piglets in a range of 0 to 14 piglets in a litter. In piglet counting and count tracking, the model achieved an average accuracy of 0.918 (R2) at an RMSE of 1.225 piglets. For the classification of an asphyxia event, the model indicated an accuracy of 0.863, specificity of 0.921, precision of 0.791, and a sensitivity of 0.723. The developed system can serve as part of Precision Livestock Farming automatic farrowing monitoring system with the aim of detecting the start of parturition, piglet count tracking, and asphyxia occurrence.

1. Introduction

In pig production and breeding, the farrowing phase is a crucial moment that heavily defines farm economics and animal welfare with regards to piglet mortality. The primary causes of losses during farrowing period are stillbirths and piglet crushing among other causes (Leenhouwers et al., 2003; Moustsen et al., 2013; Pedersen et al., 2006).

Earlier studies done by Leenhouwers et al. (2003) have reported that, globally, 0.9–1.2 piglets per litter are stillborn and deaths occurring just after parturition are often due to asphyxiation during the delivery process. Lucia et al. (2002) defined stillborn piglets as those that were apparently normal but died shortly before or during farrowing. Moreover, postmortem examination reports by Randall and Penny (1967) and Carr and Walton (1995) on stillborn piglets, estimated the time of death as during parturition period. Mild or moderate asphyxiation is a normal occurrence at the parturition phase but the level increases in offspring of polytocous species (pigs) which are born later in a litter (Herpin et al., 1996).

There are two types of asphyxiation during farrowing; fetal and prolonged asphyxia. The former results to intrapartum stillbirths while the latter results in piglets with low vitality and not necessarily stillbirth but can result in deaths during and immediately after farrowing (Herpin et al., 1996). The reduction or depletion of oxygen during farrowing results from several causes such as premature rupture of the umbilical cord, infections, piglet birth weight, sow parity, environmental factors and other dam-related factors (Leenhouwers et al., 2003; Lucia et al., 2002). Herpin et al. (1996) investigated the levels of asphyxia during sow parturition by estimating blood average partial

* Corresponding author.
E-mail address: mingxia@njau.edu.cn (M. Shen).

https://doi.org/10.1016/j.compag.2018.07.007
Received 2 May 2018; Received in revised form 1 July 2018; Accepted 3 July 2018
Available online 20 July 2018
0168-1699/

pressure of carbon dioxide (pCO_2), blood pH and lactate levels. The study established that the degree of asphyxia was directly proportional to both the birth positions in a litter and litter size, and higher in posterior births. Additionally, live born piglets in litters that underwent asphyxia have a lower vitality score and poor adaptability to the extra-uterine life, up to the age of 10 days (Oczak et al., 2016).

Asphyxiation is always predominated by the occurrence of dystocia in sows due to prolonged farrowing or weak uterine contractions which would often require birth assistance to be provided by the stockman (Pastell et al., 2014). To counter the problem of piglet mortality during the farrowing period White et al. (1996) suggested improved farrowing management protocol and by human supervision (Holyoake et al., 1995). Currently, with large-scale pig breeding, human monitoring is not feasible due to the high cost of labor and its susceptibility to negligence. Furthermore, human contact with animals increases the risks of spreading zoonotic diseases (Slingenbergh and Gilbert, 2004). With the present developments in Precision Livestock Farming (PLF) as a stockman support system in livestock management (Berckmans, 2013; Banhazi and Black, 2009), several studies have applied PLF monitoring systems with an attempt to reduce piglet mortality. Manteuffel et al. (2015) reported on the use of light barriers to detect the onset of farrowing phase in sows, Oczak et al. (2015) classified sow nesting behaviors in non-crated farrowing sows by use of accelerometers. Oczak et al. (2016) suggested an automatic piglet counter to determine the number of piglets in a pen. Nonetheless, no studies have reported on the use of PLF to detect the occurrence of asphyxia in pigs.

Stillbirth is positively related to inter-birth variation and litter size but negatively to gestation length (Björkman et al., 2017; Van Dijk et al., 2005). Thus, identification and quantification of these factors can be used as indicators to the occurrence of asphyxia. Considering that litter size is unknown before the end of farrowing, the best indicators would therefore be gestation length and inter-birth duration. This study introduces a novel technique to detect the occurrence of asphyxiation by evaluating and developing a threshold for the inter-birth interval by newborn piglets detection and count tracking in time series depth images taken during the farrowing phase. The main bottlenecks in image analysis involving livestock are often region of interest (ROI) segmentation and background removal. These problems are further complicated by the adhesive behavior of piglets (Lu et al., 2016) and the low contrast between the foreground (FG) and background (BG) (Wongsriworaphon et al., 2015). To solve the problems related to color contrast, Kongsro (2014) suggested the use of infrared (IR) depth sensors to eliminate errors associated with visible light-based sensors. Hence, this study adopted the use of such depth sensor. To accurately detect, count and count track piglets in an image it is fundamental that the adhesive piglets be split before counting.

This proposed system would significantly enhance studies and research work in evaluation and optimization of the design of farrowing facilities based on piglet detection in the determination of inter-birth duration, which will lead to improved animal welfare and maximized production. The objective of this study was to develop an IR image-based monitoring system for the farrowing process in sows, with specific objectives of developing an IR depth image processing algorithm, an efficient piglet detector, splitting of adhesive piglets and counting and count tracking algorithm. The system, when applied in a practical farm scenario, would serve as a PLF system which should provide support to Stockman as an indicator to the occurrence of possible asphyxia during the farrowing phase.

2. Materials and methods

2.1. Experimental setup

2.1.1. Animal housing and data collection

Experiments were conducted between April 2016 and April 2017 at Jurong research farm, Nanjing, Jiangsu Province, China. A total of 15 Meishan sows were included in the experiment. The sows were kept in farrowing pens of about 5 m^2 each. The floor of the pens was partially slatted plastic and partially metallic. Straw racks mountings were positioned in front of the pen near the trough, the racks were filled every morning and replenished whenever empty. The sows were fed twice a day during the experiment period. Water was provided permanently in the troughs via an automatic nipple drinker. The average temperature in the unit was 24 °C with an automatic ventilation system. The sows were introduced into the crates three days before the expected due date of parturition. The experiment period was from 3 h before the first piglet was born until the last piglet was born in the same litter.

Each pen was equipped with one top view 3D Kinect camera for Windows V2 (Microsoft Corp., Washington, USA) and a video camera DS-2CD3T35-13 (HIKVISION) connected to a Turbo digital video recorder HD DVR DS-7200HGH-SH (HIKVISION) to simultaneously monitor the pens. The cameras were installed 2.5 m perpendicularly above the pen floor. The Kinect camera was connected via a USB port to an intel core i5-4500U CPU, 4 GHz, 16 GB physical memory (Intel, Santa Clara, CA, USA), Microsoft Windows 10 PC installed with the Kinect for Windows Software Development Kit (SDK). Images were acquired from the Kinect camera using MATLAB R2016a (The MathWorks Inc., Natick, MA) software with the image acquisition Toolkit (IAT). Depth (for automatic system development) map channel (512 × 424 pixels) was selected in the AIT as shown in Fig. 1(b) for the Kinect camera. The depth images were acquired at 10 fpm and transferred to a 2 TB hard drive for subsequent analysis. The videos (for manual observation, labeling and verification) were recorded at 22 fps MOV format, and to allow for night recording, the video camera was remotely set to night mode. The Fig. 1 shows the digital color image and the corresponding depth image.

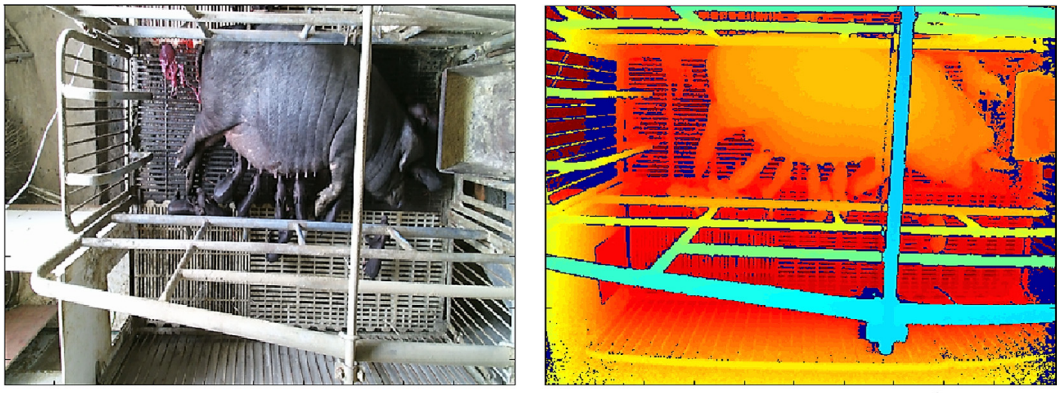

(a) (b)

Fig. 1. Captured images (a) digital color image and (b) raw depth image of a sow and piglets in a farrowing pen.

2.2. Data labeling

All the captured depth images were manually labeled by video observation based on time of parturition for each piglet and viability score (asphyxia occurrence) based on the number of times a newborn piglet attempts to stand within 1 min after birth (Herpin et al., 1996). Firstly, 1 h before the start of farrowing by each sow to account for pre-parturition (no piglets). Secondly, labeled the beginning of farrowing by each sow (the time the first piglet was born). Thirdly, labeled the time stamps of the moment of births of all remaining piglets in the litter. Fourthly, labeled the end of farrowing for each sow (the time the last piglet was born). Finally, labeled an additional 0.5 h after the end of parturition.

2.2.1. Image processing and piglet detection algorithm

The algorithms aimed at detecting the birth of each piglet in a litter, count and keep track of the piglet numbers while quantifying the inter-birth interval (*pp(t)*) (period taken to register an increase in the count). A comparison to manual observations was used to determine the accuracy of the proposed automated system. The piglet *pp(t)* was analyzed and compared to the occurrences of stillbirths and piglets' vitality score. The piglet detection algorithm was based on a parametrized multi-ellipse fitting technique. Ellipse-fitting and parameter extraction were performed on a processed depth mage.

2.2.2. Image processing algorithm

The raw depth image data was first processed as shown in Fig. 2, according to the following procedure.

Step 1. Perfumed ROI extraction by background removal (image subtraction technique).
Step 2. Since the intensities in the depth image are distances from the camera to the object (Jana, 2012), maximum and minimum thresholds were set to eliminate any remaining floor parts and the top guard rails respectively.
Step 3. Reconstructed the areas of the object that were initially blocked by the guard rails by line refilling technique.
Step 4. The resultant depth image was smoothed by Gaussian kernel filter (15 × 15 pixels zero mean) then morphological opening by a disk structural element of size 9 × 15 pixels to remove small holes to obtain a clear depth image.
Step 5. Converted the resultant image into binary image (Otsu, 1979).
Step 6. Watershed algorithm was used to segment the sow from the piglets (Meyer, 1994)
Step 7. Performed region filter on the binary image to remove the sow with reference to object area pixel threshold.

2.2.3. Piglet detection algorithm

Piglet detection was performed by a Parametrized Ellipse Fitting Algorithm (PEFA) to perform multi-ellipse fitting to an image. The number of fitted ellipses would correspond to the number of piglets in the image. Multi-ellipse fitting on an object shape was previously introduced by Panagiotakis and Argyros (2016) to fit parameter-free ellipses to 2D shapes on equal area constraint. This study proposes fitting of parametrized ellipses under an additional constraint of parameter limits while still keeping an acceptable tradeoff between the object shape coverage and Model Relative Quality (MRQ).

2.2.4. Parameter constraint

Ellipse parameter range is vital to prevent adhesive piglets being fitted as a single ellipse and part of a piglet fitted as a single ellipse (miss-fitting). A total of sixty processed images with single piglets were ellipse fitted by Direct Least Square method (Halır and Flusser, 1998). The ellipse parameters range was set based on ellipse features; major axis length *(MAAL),* minor axis length *(MIAL)* and length ratio of major and minor axis lengths *(LR)*. Of all the sixty images with single piglets fitted ellipses, the average values of *MAAL* and *MIAL* were obtained. This study applied the same methodology as that of Lu et al. (2016), to determine the maximum and minimum values of *MAAL, MIAL* and *LR* according to Eqs. (1)–(6)

$$MAAL_{MAX} = MAAL_{AV} * (1 + 0.25) \quad (1)$$

$$MAAL_{MIN} = MAAL_{AV} * (1 - 0.25) \quad (2)$$

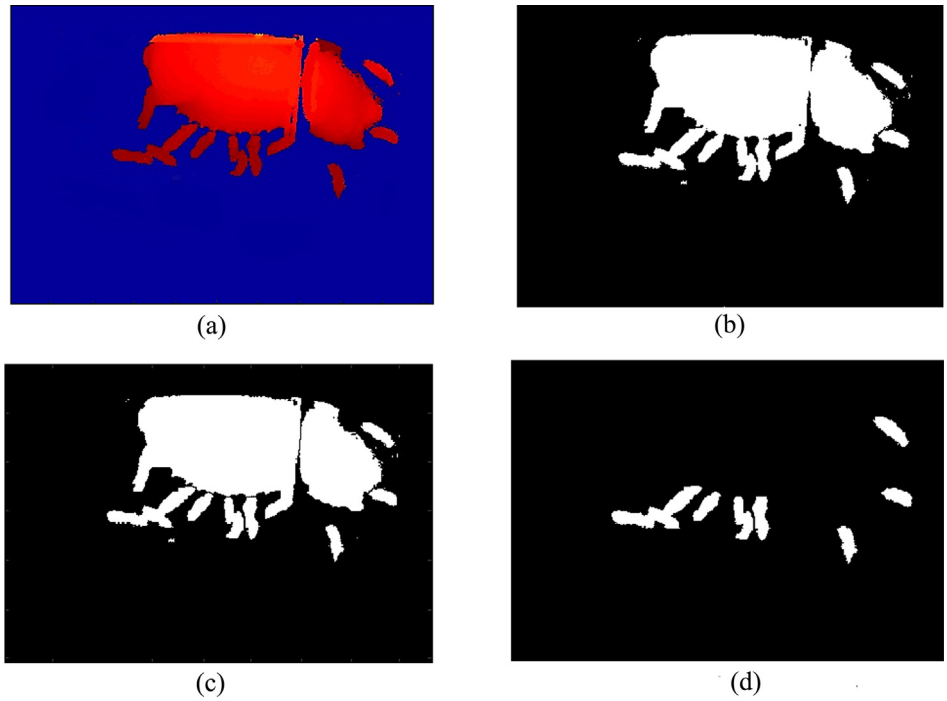

Fig. 2. Depth image processing procedure (a) background removed image (b) binarized image (c) image after watershed algorithm (d) region filtered image to remove sow image and holes filled.

$$MIAL_{MAX} = MIAL_{AV} * (1 + 0.25) \quad (3)$$

$$MIAL_{MIN} = MIAL_{AV} * (1 - 0.25) \quad (4)$$

$$LR_{MIN} = \frac{MIAL_{MIN}}{MAAL_{MAX}} \quad (5)$$

$$LR_{MAX} = \frac{MIAL_{MAX}}{MAAL_{MIN}} \quad (6)$$

The set in Eq. (7) below summarizes the parameter constraint.

$$par(E) = \{MAAL_{MAX}, MIAL_{MAX}, LR_{MAX}, MAAL_{MIN}, MIAL_{MIN}, LR_{MIN}\} \quad (7)$$

2.2.5. Equal area constraint

For a fitted set E of k ellipses E_t, to have an equal area to the object shape of area A, then the coverage of E on the object shape should be maximized to almost 100%. Consider two binary images, object shape image, and an image of the set E of k ellipses E_t. The coverage $\propto(E)$ of the ellipse set on the object shape can be defined by Eq. (8).

$$\propto(E) = \frac{1}{A}\sum_{p=1}^{n} H(p). \quad (8)$$

where A is the area of object shape (piglet image pixels), H is the intersect of the image object shape and the fitted ellipse-set E, p is the number of object shape pixels within the intersect. At maximum coverage, the area (A_E) of all the ellipses in the ellipse set E is equal to the area of the image object shape $A_E = A$. During multi-ellipse fitting by PEFA the parameters of set E of k ellipse are computed at maximum coverage (99%) to satisfy equal area criteria.

2.2.6. Image object shape analysis

Shape analysis was performed by media axis method which is a region based structural method in shape description (Zhang and Lu, 2004). Media axis transform (MAT) was determined to establish the centroids and radii of maximal circles (disks) contained within the object shape (Panagiotakis and Argyros, 2016; Zhang and Lu, 2004), this information is necessary for ellipse location and axis lengths. Shape pecstrum *pr(n)*, a morphological vector descriptor was determined from object size distribution as in Eq. (9). Shape *pr(n)* is a simple vector that describes how the area of an object is distributed. It is information non-preserving vector hence, doesn't require a lot of memory (Anastassopoulos and Venetsanopoulos, 1991).

$$pr(n) = \frac{m(I_{nB}) - m(I_{(n+1)B})}{m(I)} n = 0, 1, \cdots, k-1. \quad (9)$$

where m represents morphological image analysis, I is the binary image object shape, I_{nB} is an opening of the image I by a structural element nB. Local shape entropy S was then computed from the vector *pr(n)* by Equation (10) based on Shannon's concept of 2nd order shape entropy (Oddo, 1992). The 2nd and higher orders entropies can be used as a measure of shape complexity because they account for both spatial distributions of shape curvatures around the objects shape boundary and curvature histograms as opposed 1st order entropy which only accounts for shape curvature histograms (Oddo, 1992). This study used the 2nd order shape entropy based on computation optimization as higher order entropies (greater than 2nd order) would decrease the computation speed.

$$S = -\frac{1}{2}\sum_{1}^{n} pr(n)\ln pr(n) \quad (10)$$

2.2.7. Ellipse modeling by accelerated greedy mixture learning

The aim is to return some set E of k ellipses whose parameters lie within the *par(E)* threshold while achieving maximum coverage on the object shape. Accelerated greedy mixture learning was used because of its advantage of easier model selection due to trivial initialization and an easier escape of local maxima of the log-likelihood (Nunnink and Verbeek, 2004; 2004.). The ellipse sets are considered as models, and the task of any clustering algorithm is basically to fit a model to some data (Fit ellipses to object shape). The object shape pixels are Mixture models whose components are Gaussian density functions. Data is often assumed to be generated by a hypothetical finite Gaussian mixture defined by Eq. (11). Given that there are n image FG pixels (n components) then the Mixture will be indexed by pixel p of the FG and $f(p)$ as the distribution over the components (Nunnink and Verbeek, 2004; 2004.; McLachlan, 2000). A 2-D probability density function can then be described by Eq. (12) which defines the probability of an FG pixel to be covered by an ellipse E_t in an ellipse set of E.

$$f_h(x) = \sum_{p=1}^{n} f(x|p) f(p) \quad (11)$$

$$g_t(p) = \frac{1}{2\pi\sqrt{|c_t|}} e^{-\frac{1}{2}(p-m_t)^T C_t^{-1}(p-m_t)} \quad (12)$$

where m_t is the origin of E_t, C_t is a covariance matrix of the density function representing the eccentricity and orientation of E_t. m_{t+1} and C_{t+1} were then calculated by a greedy method by partitioning of data points and maximizing the log-likelihood of a two-component Mixture (Nunnink and Verbeek, 2004; 2004.; Verbeek et al., 2003). Similar to the study by Panagiotakis and Argyros (2016), the pixel points and the centroids were correlated to probability of any p belonging to E_t when $\frac{1}{2\pi\sqrt{|c_t|}}$ is set to unity so that all pixels at the ellipses boundary would have the same probability; hence, foreground points are clustered into k clusters G_t where $t \in [1, \ldots, k]$ by the similar rule given by Panagiotakis and Argyros (2016). The difference in this proposed study's ellipse modelling is the introduction of a limiting factor *par(E)* in the updating of E_t by the second order moments of the cluster G_t as in Eq. (13)

$$\lim_{par(E)_{min} \to par(E)_{max}} |G_t| = \pi a_t b_t. \quad (13)$$

where a_t and b_t are the major and minor axes of E_t respectively.

2.2.8. Ellipse-set selection criteria

With the ellipse parameters not being a constant value, the best suitable ellipse-set has to be computed iteratively for each image. The ellipse-sets are considered as models, and the model with the best Model Relative Quality (MRQ) was selected as the optimum set to represent the object shape. Akaike Information Criterion (AIC) was used to compute the MRQ (Wagenmakers and Farrell, 2004) as given by Eq. (14). Previous studies have also preferred AIC to other information criterion like the Bayesian Information Criterion (BIC) due to over-fitting problem (Panagiotakis and Argyros, 2016; Wagenmakers and Farrell, 2004; Burnham and Anderson, 2003).

$$AIC = SIn(1 - \alpha(E)) + 2k \quad (14)$$

where S is the sample size in a lossless representation of the object shape (shape entropy). $(1 - \alpha(E))$ is the coverage error and k is the number of estimated parameters in the model. Given a set of models for the data, the preferred model is one with the minimum AIC value (minimization of the quantity) (Burnham and Anderson, 2003).

2.2.9. Parametrized ellipse fitting algorithm

This algorithm aims at modeling the object shape by a set of ellipses, it starts by fitting maximum number of ellipses and iteratively decreases the number to achieve $A_E = A$ and $par(E)$ criterions. The initial number of fitted ellipses depends on the selected number of centroids in the MAT. The final ellipse set E is selected based on the MRQ. The algorithm is summarized below and by flow chat in Fig. 3.

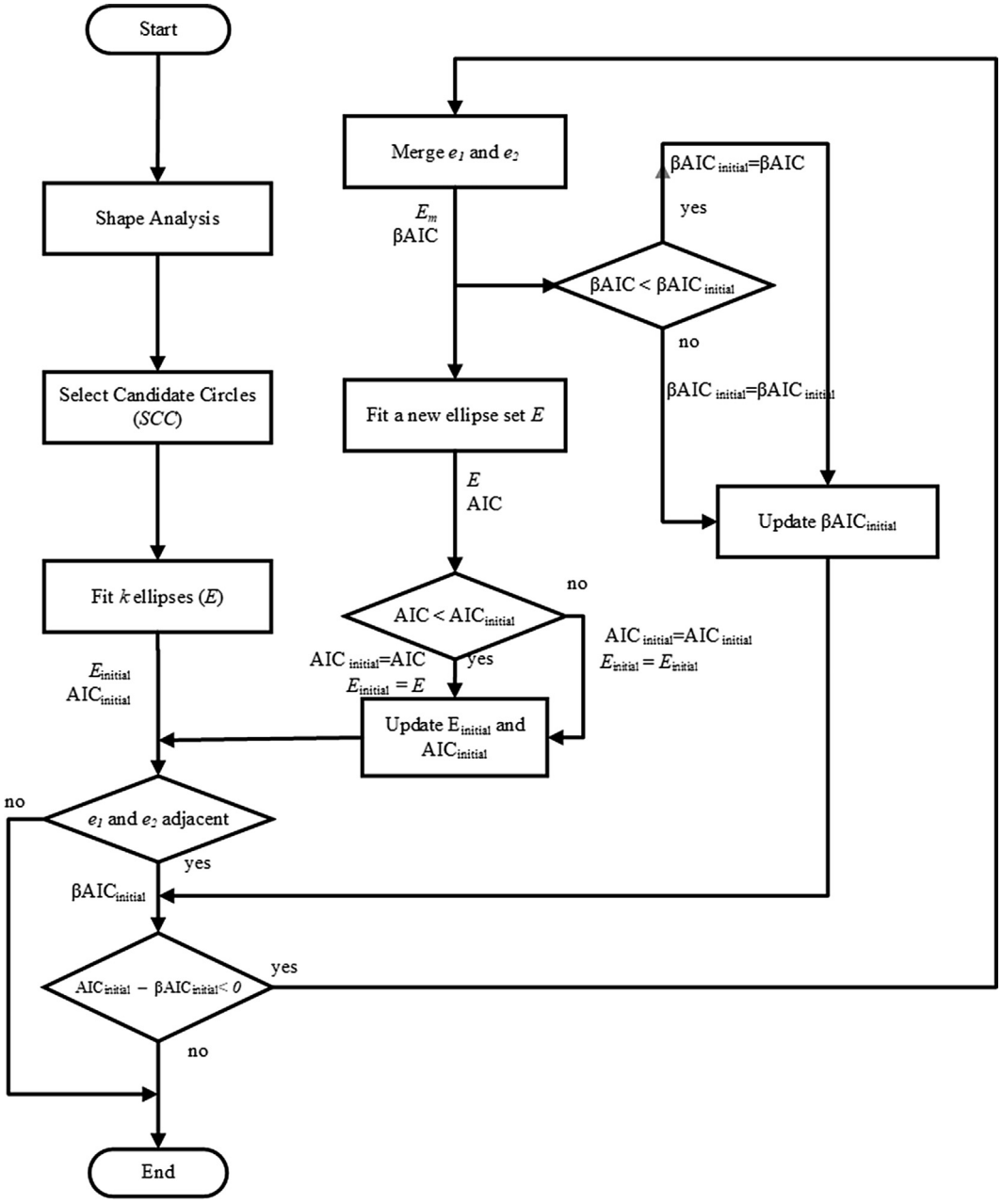

Fig. 3. Flowchart of the parametrized ellipse fitting algorithm.

```
[C, R, pr, S] = ShapeAnalysis(I)
CC = ExtractCandidateCircles(C, R)
SCC = SelectCandidateCircles(CC, par(E))
k = |SCC|
E = AGEM-GMM (I, SCC, k, par(E))
AIC_initial = FindModelAIC(I, E, S)
while (k ≠ 1)
  for e1, e2 ∈ E
    βAIC_initial(e1, e2) = ∞ where ∀ e ∈ E
    If e1 and e2 are adjacent
      while AIC_initial − βAIC_initial(e1, e2) < 0
        Em = AGEM-GMMmerge(E, e1, e2, par(E))
        βAIC(e1, e2) = FindModelAIC (I, S, Em)
        E = AGEM-GMM (I, Em, k, par(E))
        AIC = FindModeAIC (I, E, S)
        If βAIC(e1, e2) < βAIC_initial(e1, e2)
          βAIC_initial(e1, e2) = βAIC(e1, e2)
        end
        If AIC < AIC_initial
          AIC_initial = AIC
          E = E
        end
      end
    end
  end
  k = k − 1
end
```

Shape analysis performed on the input object shape binary image *I*, returned the maximal circle centers *C* and their radii *R*, the shape pecstrum *pr(n)* and shape entropy *S*. The *C*s are then used to compute the candidate circles *CC* that represents *I*. Two criterions are followed to minimize *CC*. Firstly, the circles of the selected *CC* (*SCC*) should not overlap each other and secondly, the radii of the circles should be

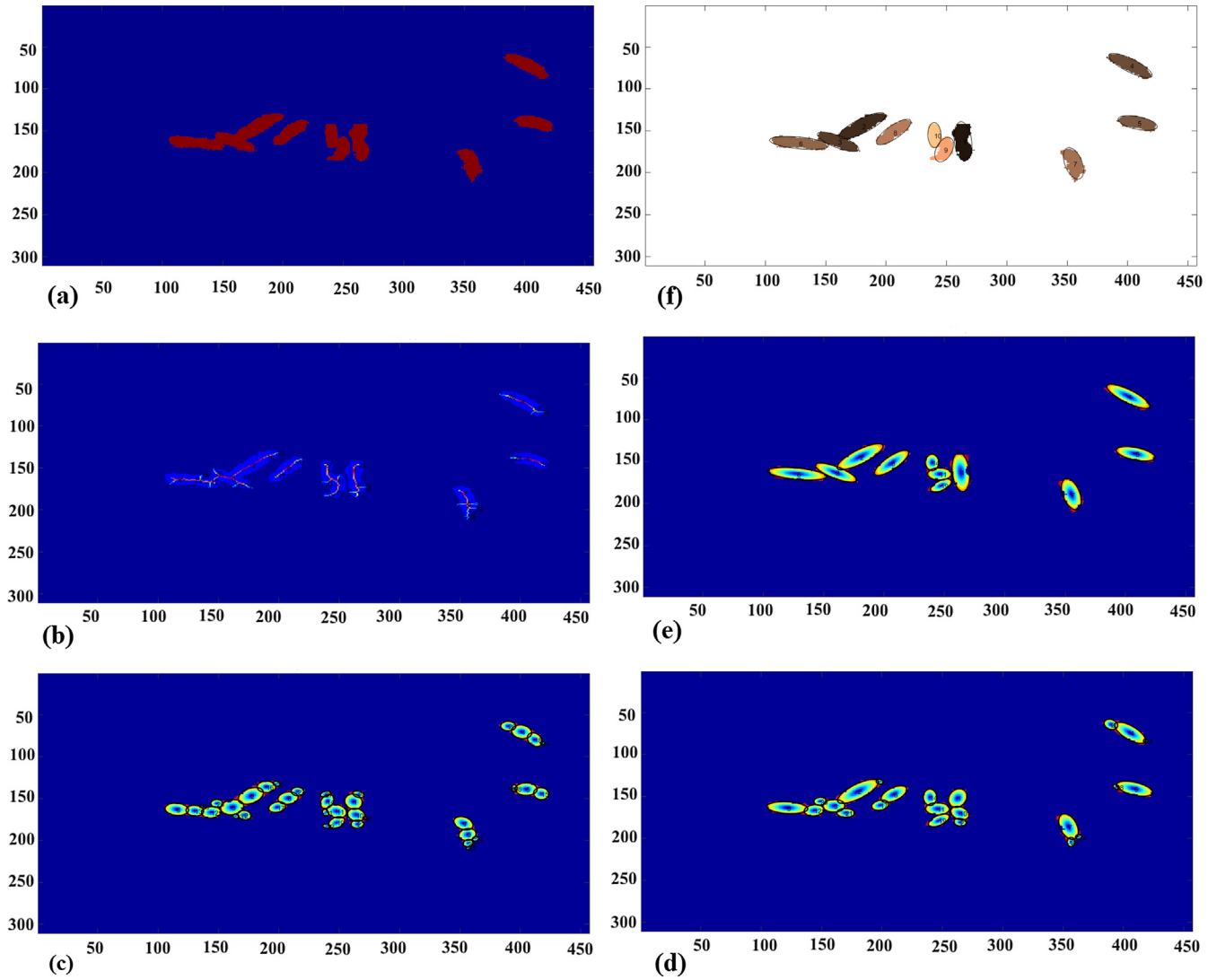

Fig. 4. PEFA flow for multiple ellipse-fitting (a) the input binary image I (b) computation of MAT (Centroid Points = 26) and shape entropy (S = 16.89) (c) fitting of initial number of ellipses (SCC = 38) (d) merging of adjacent ellipses in adherence to ellipse parameter and coverage constraints (e) continual of merging of adjacent ellipses (f) final ellipse fit for the image (k = 10 = number of piglets).

within 50% of the maximum and minimum thresholds values set by the *par(E)* constraint. The *SCC* is *k* selected circles, the maximum number of ellipses are computed at $k = SCC$ by the Accelerated Greedy Expectation Maximization Algorithm for Gaussian Mixture Model (AGEM-GMM) and similarly the initial AIC of the computed ellipse set *E*. In the iteration loop, a pair of adjacent ellipses in the ellipse set are selected for merging with the aim of decreasing the AIC. The adjacent ellipses e_1 and e_2 are merged by AGEM-GMM without affecting other ellipses in the set *E* resulting in a new ellipse set E_m. The AIC of E_m ($\beta AIC(e_1, e_2)$) is then computed on the defined *S*. AGEM is again initialized to update the entire ellipse parameters to return a new set *E*. The new AIC is computed based on the new *E*, which is then compared to the initial AIC, if its lower than the initial AIC the $AIC_{initial}$ is updated similarly to the $\beta AIC(e_1, e_2)$. The difference between the $\beta AIC(e_1, e_2)$ and the $AIC_{initial}$ is determined, and the iteration stops when this difference becomes positive as AIC is a minimization of quantity, thus, low values indicated suitable merging. Fig. 4 shows the performance flow of the PEFA on an image object.

Table 1
The number of piglets born, number of stillbirths and farrowing duration of each sow.

Sow reference number	Number of piglets born	Number of stillbirths	Number of crushes	Farrowing duration (h)
Sow TEFG1	14	0	1	2.6
Sow TEFG2	10	0	0	1.9
Sow TEFG3	13	1	0	2.9
Sow TEFG4	12	0	0	2.1
Sow TEFG5	13	0	0	2.5
Sow TEFG6	14	0	0	2.3
Sow TEFG7	10	0	0	2.1
Sow TEFG8	12	0	0	2.4
Sow TEFG9	14	1	0	2.8
Sow TEFG10	13	0	0	2.2
Sow TEFG11	9	0	0	2.0
Sow TEFG12	12	0	0	1.9
Sow TEFG13	11	0	0	2.2
Sow TEFG14	13	0	0	2.7
Sow TEFG15	14	3	0	3.4
Total	184	5	1	36.0

3. Results

The behavior of 15 sows was labeled and tested on the proposed

Table 2
Parameter range of ellipse fitted by direct least square method on images with a single piglet.

Range of MAAL	Range of MIAL	Range of LR
35–49	13–16	0.27–0.46

algorithms. The sows gave birth to a total of 184 piglets at a total farrowing duration of 36.0 h as shown in Table 1. Stillbirths occurred in 3 litters. Of the total piglets born 5 (2.7%) were stillborn, and 1 (0.5%) died due to crushing as shown in Table 1.

Manual labeling confirmed that all the images were correctly captured at 10 fpm by image acquisition. In ellipse parameter range computation, sixty images with single piglets were randomly selected. The computed average parameter ranges are presented in the Table 2 (note that all images were taken just after birth).

3.1. Algorithm evaluation

The object shape entropy S of all the images were computed, different images returned different values of S. A higher value of S indicates a more complex object shape image. It was observed that as the number of piglets increased the higher the S as shown in Fig. 5.

Fig. 6 presents the piglet counting plots of 4 sows by both observation and proposed algorithm from the time of start of the experiment to the end. It's worth noting that Sow TEFG3 had the highest accuracy (R2) of 0.975 with an RMSE of 0.752 piglets. Sow TEFG11 had the lowest accuracy of 0.844 with an RMSE 1.256 Piglets as from Table 4. The average count detection accuracy per label by the PEFA is presented in Table 3. From the Table 3 and Fig. 6, the false positive detection at the start of the experiment occurred due to the detection of the sow's leg as a piglet, due to incomplete line filling or incorrect watershed in some images when the sow's leg was at the same height from the camera as the piglets during side-lying. Additionally, the sharp drop in the piglet count at some instance as was observed in Fig. 6 was due to some piglets being on top of the sow at the time of image capturing.

3.2. Piglet counting, count tracking, and inter-birth interval evaluation

Piglet counting was achieved by registering only sequential increments in the piglet count by one piglet while ignoring non-sequential increases (increases by more than one piglet) and any count decrements in each farrowing phase. This study established an average counting accuracy of 0.918 (R2) and an RMSE of 1.225 piglets per sow as shown in Table 4. By observation and proposed piglet detection algorithm, the mean $pp(t)$ of all the sows were analyzed as presented in Fig. 7.

By manual verification the following observations were made: the mean $pp(t)$ increases with litter capacity, $pp(t)$ had a large variation as from the 10th interval to the last, the longest periods occurred at the 10th and 13th interval. The 1st interval and the last interval durations were long with the last being longer. The middle intervals had considerably shorter durations that occurred randomly from the 2nd to the 9th interval. The mean computed $pp(t)$ as shown in Fig. 7 above had the same trend as the observed except in the 1st inter-birth duration due to the detection of sow's leg as a piglet in some images before farrowing began.

The Fig. 8 above shows the comparison between the observed and proposed system on the $pp(t)$ for some sows. The peak points correspond to long inter-birth durations and stillbirths in Sow TEFG3 and Sow TEFG15. The peak at the 1st interval in Sow TEFG8 and Sow TEFG11 were due to detection of sow leg as piglet before the start of parturition. All the last intervals can be considered at peaks because they are higher than the mid-intervals. Based on the mean of the observed minimum $pp(t)$ with the occurrence of stillbirth and the maximum $pp(t)$ without the occurrence of stillbirth in the entire dataset, an alarm threshold was set at 21 min. Fig. 8 shows the alarms generated on algorithm testing. It was noted that the alarms corresponded to the peak points. A confusion matrix in Table 5 shows the statistical measures of the performance of the asphyxia occurrence detector classifier using the criteria accuracy = (TP + TN)/(TP + TN + FP + FN), specificity = TN/(TN + FP), precision = TP/(TP + FP) and sensitivity = TP/(TP + FN); where TP is True Positive, TN is True Negative, FP is False Positive and FN is False Negative. The result of the classification achieved an accuracy of 0.863, specificity of 0.921, precision of 0.791, and a sensitivity of 0.723.

4. Discussions

4.1. Algorithms analysis

This study introduces a novel methodology of the use of IR depth sensor in farrowing monitoring. Firstly, image processing algorithm was developed to perform ROI extraction (piglet image shape) on the depth image. Depth images are more preferred in situations where ambient light variation would largely affect accuracy. Additionally, visible light-based image processing results to the arduous task of background removal (Kongsro, 2014), consider in this study the FG has an almost equal color intensity as the BG. Secondly, a parameterized ellipse fitting algorithm was used to count, track piglet count in an image and quantify the $pp(t)$. The proposed algorithm computation speed was observed to increase as S increased because S is directly proportional to the number of piglets as more piglets introduce more shape structures in the image. Additionally, S as a measure of object shape complexity, thus, it's logarithmically directly proportional to scale due to increased shear transformation (Panagiotakis and Argyros, 2016). The algorithm returned different quantity ellipse-sets, the best set was selected based on MRQ by AIC.

4.2. Piglet detection and counting

Piglet counter during farrowing was previously reported by Oczak et al. (2016) by use of a transfer transform model and image feature extraction methodology to count the number of piglets in a pen. This proposed study introduces a novel method that takes into account the adhesive behavior of piglets due to their social nature by splitting of adhesive piglets methodology. Several studies have been reported on splitting and counting of occluded objects, Song et al. (2014) reported on the use of color images to locate and count pepper fruits of complex shapes and varying colors. Font et al. (2014) presented a procedure of counting red grapes by detecting specular spherical reflection peaks in color images taken at night using artificial illumination. Pastrana and Rath (2013) presented a solution for the detection of partially occluded plantlets by use of active shape models. Despite the successes of the methods mentioned above, they mainly depended on color and shape descriptions to split adhesive objects, thus, cannot be applied in non-color images, varying ambient light conditions and non-regular shaped image objects. A study by Lu et al. (2016) suggested the use of ellipse shape feature to automatically splitting adhesive piglets in grayscale image by multi-ellipse fitting by chain code representation. This method, however, suffered from complicated spatial relationship of piglets as the number of piglets increased, leading to extraction of false representative concave points, thus, counting accuracy worsens as the number of piglets increases. This study introduces PEFA that takes into account both the region and contour-based shape descriptions. From the Table 3, the count detection accuracy is independent of the number of piglets but only depend on the input binary image features. It can be concluded that for accurate multi-ellipse fitting for partially occluded object shape, the best practice would be to apply both region and contour shape descriptors.

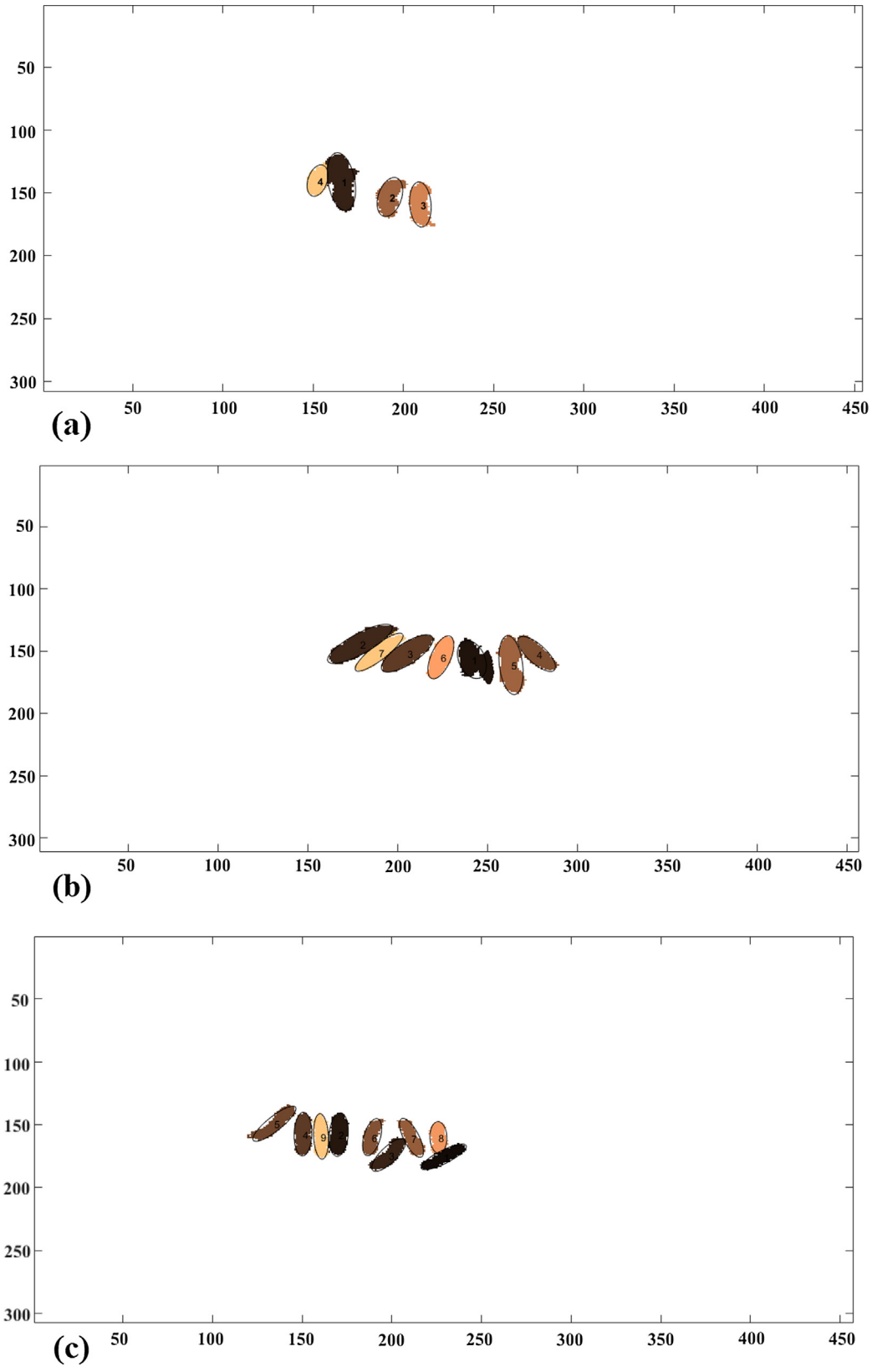

Fig. 5. Ellipse fitting to detect different number of piglets (a) S = 6.81, SCC = 12 and k = 4 (b) S = 9.64, SCC = 28 and k = 7 and (c) S = 12.96, SCC = 31 and k = 9.

4.3. Asphyxia occurrence detection

An inter-birth interval threshold was established at 21 min after performing the experiments. This concurs with studies done by Klocek et al. (1992), Hoy and Lutter (1995) and Van Dijk et al. (2005) who reported an inter-birth interval range of 15.2–22.4 min in sows. From the Fig. 7 above, the long *pp(t)* 10, 12 and 13 coincided with the occurrence of stillbirths by sows TEFG3 (interval 10 – 11), sow TEFG9 (12

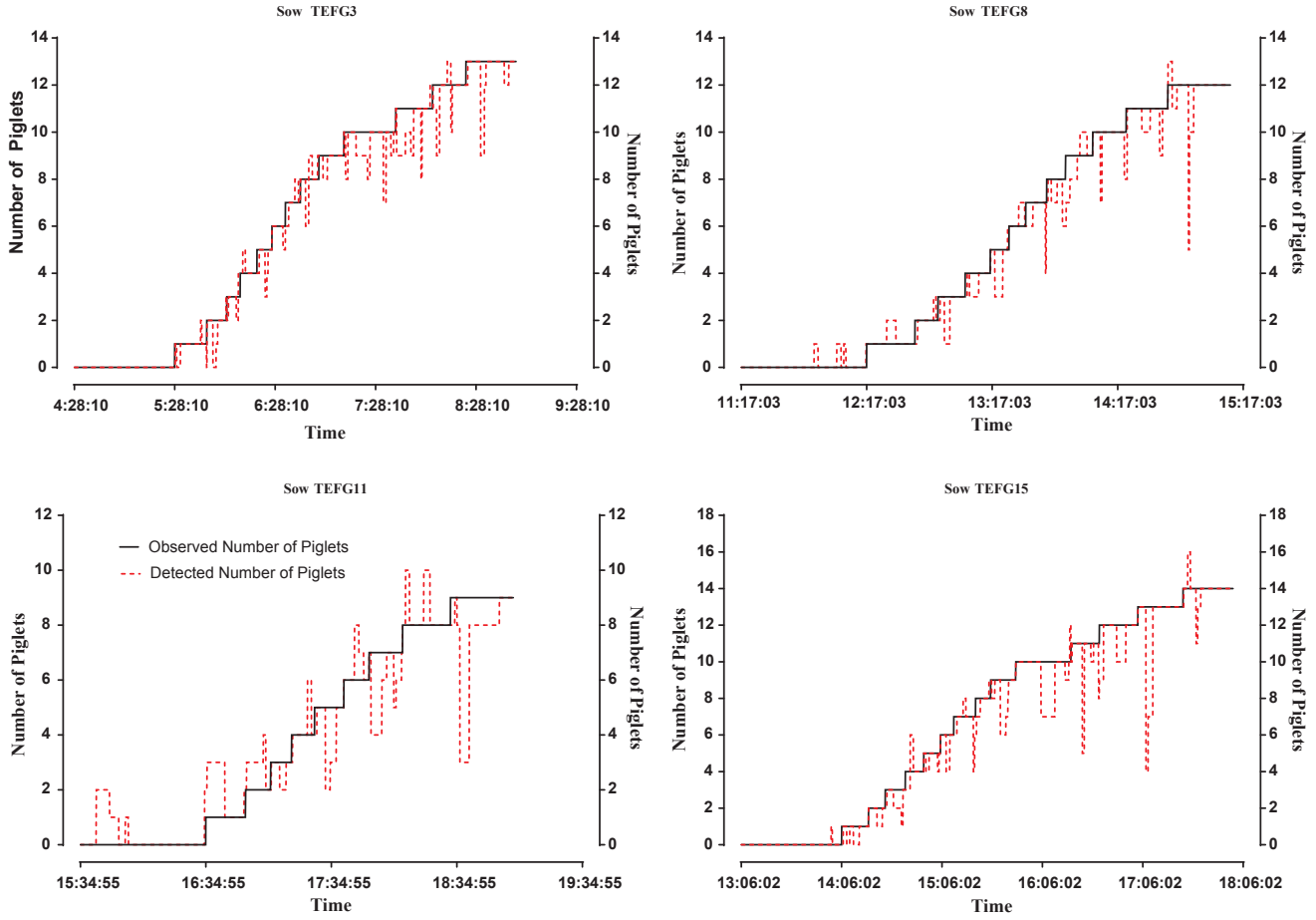

Fig. 6. Piglet count tracking by observation and the developed piglet detection algorithm.

Table 3
The average count detection accuracy of the proposed algorithm.

Labeled number of piglets	Average Accuracy of piglet detection
0	0.832
1	0.829
2	0.736
3	0.702
4	0.731
5	0.776
6	0.698
7	0.728
8	0.787
9	0.820
10	0.739
11	0.712
12	0.699
13	0.755
14	0.801

Table 4
The model performance for each sow.

Sow reference number	Accuracy (R2)	RMSE
Sow TEFG1	0.910	1.621
Sow TEFG2	0.895	0.858
Sow TEFG3	0.975	0.752
Sow TEFG4	0.922	1.291
Sow TEFG5	0.951	0.892
Sow TEFG6	0.899	1.927
Sow TEFG7	0.900	0.960
Sow TEFG8	0.974	0.727
Sow TEFG9	0.928	1.161
Sow TEFG10	0.897	0.982
Sow TEFG11	0.844	1.256
Sow TEFG12	0.913	1.329
Sow TEFG13	0.931	1.416
Sow TEFG14	0.889	2.001
Sow TEFG15	0.944	1.203
Average	0.918	1.225

– 13) and sow TEFG15 (10 – 11, 12 – 13, 13 – 14). This finding is supported by Van Dijk et al. (2005) and Lucia et al. (2002) who reported that stillborn piglets are always born after a significantly longer *pp(t)* than the liveborn in the same litter. These are large litter sizes as per this dataset. Herpin et al. (1996) established that the average blood pCO_2 increases with litter size, thus the stillbirths most likely resulted from asphyxiation. Additionally, it was observed that Sow TEFG12 had a posterior birth of its last piglet (11 – 12). This *pp(t)* was longer and even though it was a liveborn, the piglet was observed to have a low vitality. Piglets born late after others in the same litter always have a longer *pp(t)* and a higher degree of asphyxia and would have a low survival rate within a few days after birth (Herpin et al., 1996; Van Dijk et al., 2005). The occurrence of stillborn in a litter is an additional indicator of low endurance of the liveborn within the same litter (Oczak et al., 2016); this was observed in Sow TEFG3 after stillbirth (10 – 11) where the next born piglet showed low vitality that required extra care and attention. The 1st *pp(t)* was higher than mid *pp(t)* (before the 10th interval). The same was reported by Van Dijk et al. (2005), who established that this was due to the secretion patterns of oxytocin during parturition which increases after the birth of the first piglet but start to decrease after about 1 h (Lawrence et al., 1995).

As previously mentioned, piglet crushing is also a significant cause of high piglet mortality during the farrowing phase. The occurrence of

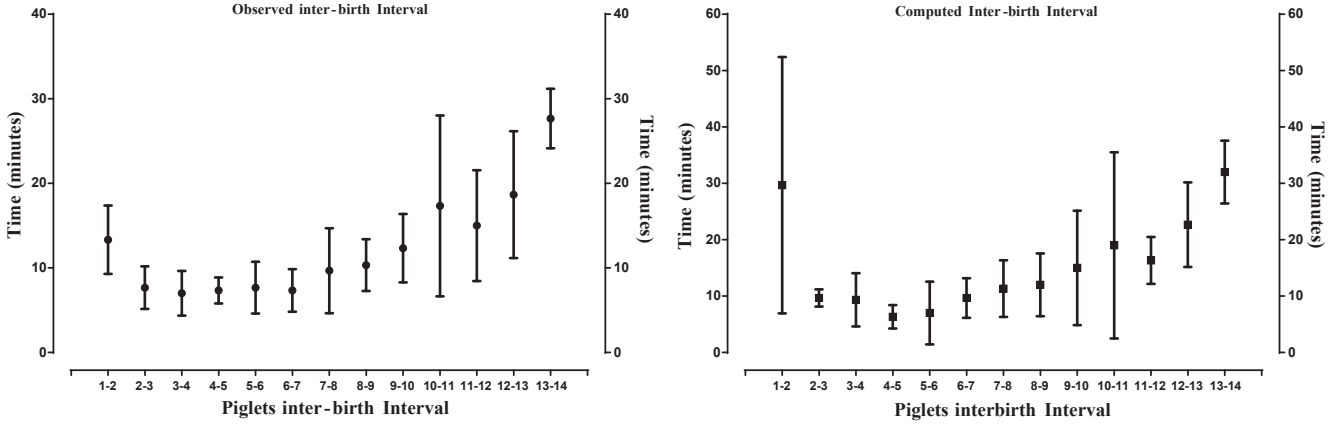

Fig. 7. A comparison of the inter-birth interval between manual observation and proposed piglet detector computation.

asphyxia in a litter would influence the event of crushing, piglets with low vitality are always weak hence cannot move away from the sow, thus, increased risk of being crushed. Specific management procedures should be implemented when asphyxia occurrence is detected. Herpin et al. (2001) suggested the use of oxygen inhalation at birth, while Oczak et al. (2016) suggested on obstetric intervention when the *pp(t)* exceeded a specific threshold. This study agrees with the latter recommendation due to high costs involved in the supply of oxygen, but evaluation of *pp(t)* would be a sufficient indicator prior to or during the occurrence of asphyxiation.

Birth detection devices have long been introduced and used to detect parturition. Some of these devices are attached to the animal vulva to generate a signal during parturition (Berry, 2002). Sound analysis method proposed by De Wit and Bouma (1987) at farrowing pens detected piglets after birth and could also detect piglet crushing. Labrecque et al. (2014) proposed the use of infrared temperature

Table 5
A confusion matrix for the classification of Asphyxia occurrence by alarm threshold.

Asphyxia occurrence	Alarm		Total
	Yes	No	
Yes	34	9	43
No	13	105	118

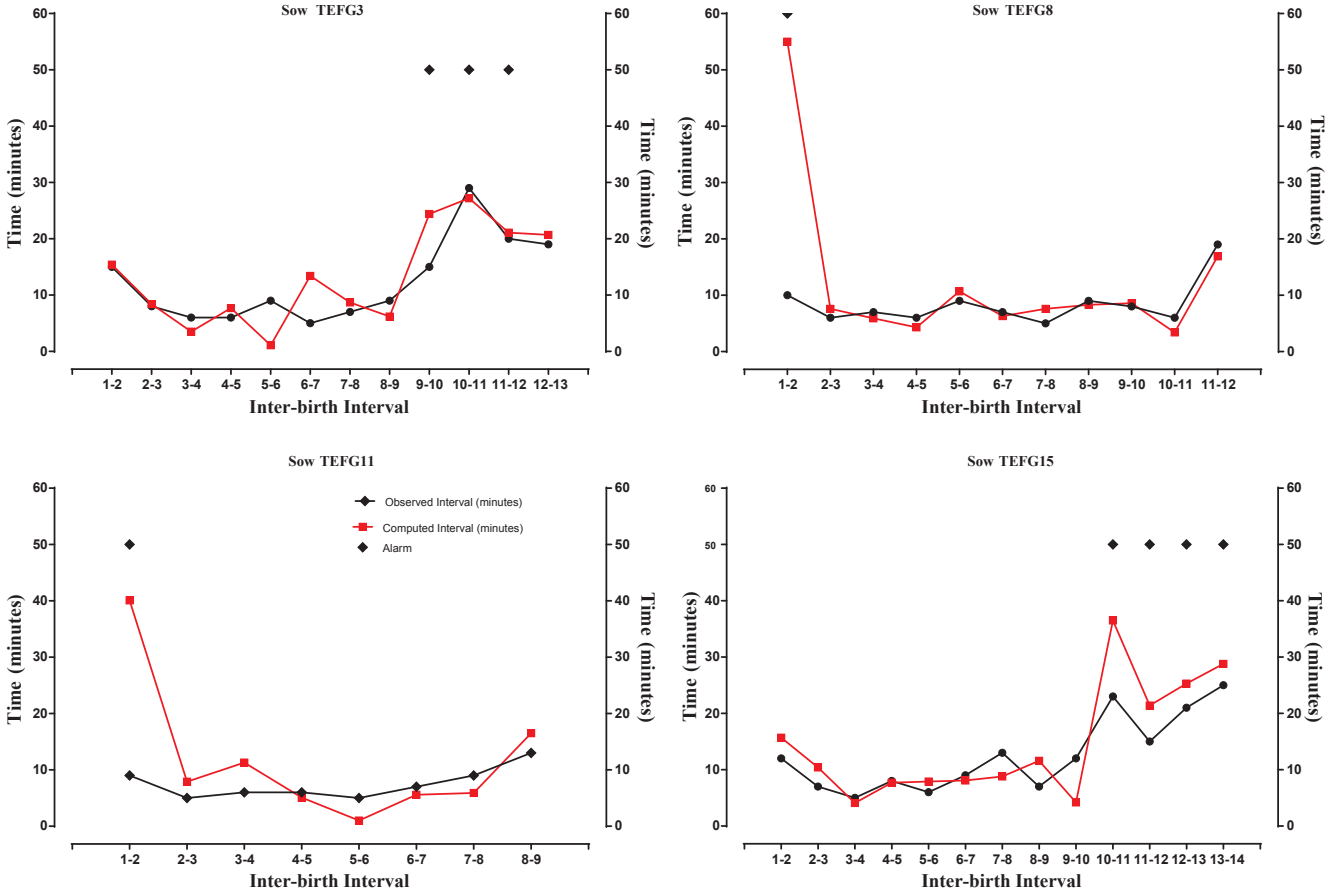

Fig. 8. The inter-birth duration by observation and by the developed piglet detector.

sensors to detect piglet presence. Some of these approaches, however, required contact with the sow, while others required extensive data processing to eliminate data redundancy in sound, weight and motion analysis and also experienced transmission delays by the Wireless sensor network. Thus, compromising real time detection or induce animal stress by contact sensors. Studies based on sow behavioral analysis have also attempted to predict the occurrence of parturition (Manteuffel et al., 2015; Oczak et al., 2015; Aparna et al., 2014), but up to now no scientific reports have been made that have satisfactory predicted the start of farrowing in sows. By utilizing this proposed method, it is possible to automatically and precisely detect the birth of every piglet in a litter non-intrusively without disturbing the sows. Hence, the stockman can be alerted when the first piglet is born. Additionally, this proposed system can perform non-intrusive piglet counting and count tracking in adhesive conditions and also determine the duration of farrowing in sows.

Factors such as sow parity, litter birth weight (Lucia et al., 2002), post-partum behaviours (Minick et al., 1997) and gestation period (Van Dijk et al., 2005) have been reported to be indicators to occurrences of stillbirths in a sow. Currently, there are no literature predicting asphyxia or stillbirths in sows. Thus, with the application of this developed monitoring system based on the discussed approach, the start of parturition and the occurrence of asphyxiation can be precisely detected during the farrowing phase in sows. This technique can be used as a PLF system to reduce surveillance costs, benefiting both animal welfare and boosting farm productivity.

5. Conclusions

This study proposes a piglet detection system based on depth image analysis and PEFA to detect, count, track the number and perform *pp(t)* evaluation with the aim of detecting the occurrence of asphyxiation. The main drawback exhibited by the proposed system is that the study did not consider images with large overlapping piglets (crowed piglets or completely occluded piglets). However, this methodology with acceptable accuracies achieved the objectives of this research study. Thus, it has a potential to be applied as a PLF monitoring system for the entire farrowing phase in sows as a measure to lower perinatal mortality in piglets. Additionally, this system could establish the exact time of birth of each piglet, piglets birth order, litter size, and sow farrowing duration non-intrusively. The application of this system in farms would provide timely interventions to be carried out in combating piglet mortality asphyxiation related loses. This should improve both animal welfare and farm economy.

Acknowledgments

All experiments were carried out in Nanjing Agricultural University facilities, in compliance with and using protocols approved by the biosafety committee of Nanjing Agricultural University. The handling of the Meishan sows was performed in accordance with the guidelines approved by the experimental animal administration and ethics committee of Nanjing Agricultural University. The project was funded by China National Key Research and Development project (Grant No. 2017YFD0701602-2).

References

Anastassopoulos, V., Venetsanopoulos, A., 1991. The classification properties of the pecstrum and its use for pattern identification. Circuits, Syst. Signal Process. 10 (3), 293–326.
Aparna, U., Pedersen, L.J., Jørgensen, E., 2014. Hidden phase-type Markov model for the prediction of onset of farrowing for loose-housed sows. Comput. Electron. Agric. 108, 135–147.
Banhazi, T., Black, J.L., 2009. Precision livestock farming: a suite of electronic systems to ensure the application of best practice management on livestock farms. Australian J. Multi-disciplinary Eng. 7 (1), 1–14.
Berckmans, D., 2013. Basic principles of PLF: gold standard, labelling and field data. In: The 6th European Conference on Precision Livestock Farming, pp. 21–29.
Berry, D.K., 2002. Amniotic Fluid Alerting Device. Google Patents.
Björkman, S., Oliviero, C., Rajala-Schultz, P., Soede, N., Peltoniemi, O., 2017. The effect of litter size, parity and farrowing duration on placenta expulsion and retention in sows. Theriogenology 92, 36–44.
Burnham, K.P., Anderson, D.R., 2003. Model Selection and Multimodel Inference: A Practical Information-Theoretic Approach. Springer Science & Business Media.
Carr, J., Walton, J., 1995. Recognising the stillborn piglet. Pigs 11, 30–31.
De Wit, P.A., Bouma, J., 1987. Apparatus for Preventing Shoats from Being Crushed to Death in Hog Breeding Operations and the Use Thereof as a Device for Indicating the Start of the Dam's Birthing Procedure. Google Patents.
Font, D., Pallejà, T., Tresanchez, M., Teixidó, M., Martinez, D., Moreno, J., Palacín, J., 2014. Counting red grapes in vineyards by detecting specular spherical reflection peaks in RGB images obtained at night with artificial illumination. Comput. Electron. Agric. 108, 105–111.
Halır, R., Flusser, J., 1998. Numerically stable direct least squares fitting of ellipses. In: Proc 6th International Conference in Central Europe on Computer Graphics and Visualization WSCG, pp. 125–132.
Herpin, P., Le Dividich, J., Hulin, J.C., Fillaut, M., De Marco, F., Bertin, R., 1996. Effects of the level of asphyxia during delivery on viability at birth and early postnatal vitality of newborn pigs. J. Animal Sci. 74 (9), 2067–2075.
Herpin, P., Hulin, J., Le Dividich, J., Fillaut, M., 2001. Effect of oxygen inhalation at birth on the reduction of early postnatal mortality in pigs. J. Animal Sci. 79 (1), 5–10.
Holyoake, P.K., Dial, G.D., Trigg, T., King, V.L., 1995. Reducing pig mortality through supervision during the perinatal period. J. Animal Sci. 73 (12), 3543–3551.
Hoy, S., Lutter, C., 1995. Effect of housing of sows during parturition and the vitality of the piglets. Tierarztliche Praxis 23 (4), 367–372.
Jana, A., 2012. Kinect for windows SDK programming guide: Packt. Publishing Ltd.
Klocek, vC., Ernst, E., Kalm, E., 1992. Geburtsverlauf bei Sauen und perinatale Ferkelverluste in Abhängigkeit von Genotyp und Haltungsform. Züchtungskunde 64 (2), 121–128.
Kongsro, J., 2014. Estimation of pig weight using a Microsoft Kinect prototype imaging system. Comput. Electron. Agric. 109, 32–35.
Labrecque, S., Labrecque, R., Labrecque, G., 2014. Birth Monitoring and Heating System for Piglets. Google Patents.
Lawrence, A., Petherick, J., McLean, K., Deans, L., Chirnside, J., Vaughan, A., Gilbert, C., Forsling, M., Russell, J., 1995. The effects of chronic environmental stress on parturition and on oxytocin and vasopressin secretion in the pig. Animal Reprod. Sci. 38 (3), 251–264.
Leenhouwers, J., Wissink, P., Van der Lende, T., Paridaans, H., Knol, E., 2003. Stillbirth in the pig in relation to genetic merit for farrowing survival 1. J. Animal Sci. 81 (10), 2419–2424.
Lu, M., Xiong, Y., Li, K., Liu, L., Yan, L., Ding, Y., Lin, X., Yang, X., Shen, M., 2016. An automatic splitting method for the adhesive piglets' gray scale image based on the ellipse shape feature. Comput. Electron. Agric. 120, 53–62.
Lucia Jr, T., Corrêa, M.N., Deschamps, J.C., Bianchi, I., Donin, M.A., Machado, A.C., Meincke, W., Matheus, J.E., 2002. Risk factors for stillbirths in two swine farms in the south of Brazil. Prevent. Veterinary Med. 53 (4), 285–292.
Manteuffel, C., Hartung, E., Schmidt, M., Hoffmann, G., Schön, P.C., 2015. Towards qualitative and quantitative prediction and detection of parturition onset in sows using light barriers. Comput. Electron. Agric. 116, 201–210.
McLachlan, G., Peel, D., 2000. Finite Mixture Models, Willey Series in Probability and Statistics. John Wiley & Sons, New York.
Meyer, F., 1994. Topographic distance and watershed lines. Signal Process. 38 (1), 113–125.
Minick, J.A., Lay, Jr. D., Ford, S.P., Hohenshell, L., Biensen, N.J., Wilson, M., 1997. Differences in Maternal Behavior between Meishan and Yorkshire Gilts.
Moustsen, V., Hales, J., Lahrmann, H., Weber, P.M., Hansen, C.F., 2013. Confinement of lactating sows in crates for 4 days after farrowing reduces piglet mortality. Animal 7 (4), 648–654.
Nunnink, J., Verbeek, J., Vlassis, N., 2004. Accelerated greedy mixture learning. In: Benelearn: Annual Machine Learning Conference of Belgium and the Netherlands.
Oczak, M., Maschat, K., Berckmans, D., Vranken, E., Baumgartner, J., 2015. Classification of nest-building behaviour in non-crated farrowing sows on the basis of accelerometer data. Biosystems Eng. 140, 48–58.
Oczak, M., Maschat, K., Berckmans, D., Vranken, E., Baumgartner, J., 2016. Automatic estimation of number of piglets in a pen during farrowing, using image analysis. Biosystems Eng. 151, 81–89.
Oddo, L.A., 1992. Global shape entropy: a mathematically tractable approach to building extraction in aerial imagery. In: The 20th AIPR Workshop: Computer Vision Applications: Meeting the Challenges. International Society for Optics and Photonics, pp. 91–102.
Otsu, N., 1979. A threshold selection method from gray-level histograms. IEEE Trans. Systems, Man, Cybernet. 9 (1), 62–66.
Panagiotakis, C., Argyros, A.A., 2016. Parameter-free modelling of 2D shapes with ellipses. Pattern Recogn. 53, 259–275.
Pastell, M., Hietaoja, J., Tiusanen, J., Yun, J., Valros, A., 2014. A model to detect farrowing based on sow activity. In: Proceedings International Conference of Agricultural Engineering, Zürich, 06-1007 2014: Geyseco.
Pastrana, J.C., Rath, T., 2013. Novel image processing approach for solving the overlapping problem in agriculture. Biosystems Eng. 115 (1), 106–115.
Pedersen, L.J., Jørgensen, E., Heiskanen, T., Damm, B.I., 2006. Early piglet mortality in loose-housed sows related to sow and piglet behaviour and to the progress of parturition. Appl. Animal Behav. Sci. 96 (3), 215–232.
Randall, G., Penny, R., 1967. stillbirths in pigs-possible role of anoxia. Veterinary Rec. 81 (14), 359–1000.

Slingenbergh, J., Gilbert, M., Balogh, K.D., Wint, W., 2004. Ecological sources of zoonotic diseases. Revue scientifique et technique-Office international des épizooties 23 (2), 467–484.
Song, Y., Glasbey, C., Horgan, G., Polder, G., Dieleman, J., Van der Heijden, G., 2014. Automatic fruit recognition and counting from multiple images. Biosystems Eng. 118, 203–215.
Van Dijk, A., Van Rens, B., Van der Lende, T., Taverne, M., 2005. Factors affecting duration of the expulsive stage of parturition and piglet birth intervals in sows with uncomplicated, spontaneous farrowings. Theriogenology 64 (7), 1573–1590.
Verbeek, J.J., Vlassis, N., Kröse, B., 2003. Efficient greedy learning of Gaussian mixture models. Neural Comput. 15 (2), 469–485.
Wagenmakers, E., Farrell, S., 2004. AIC model selection using Akaike weights. Psychonom. Bull. Rev. 11 (1), 192–196.
White, K., Anderson, D., Bate, L.A., 1996. Increasing piglet survival through an improved farrowing management protocol. Canadian J. Animal Sci. 76 (4), 491–495.
Wongsriworaphon, A., Arnonkijpanich, B., Pathumnakul, S., 2015. An approach based on digital image analysis to estimate the live weights of pigs in farm environments. Comput. Electron. Agric. 115, 26–33.
Zhang, D., Lu, G., 2004. Review of shape representation and description techniques. Pattern Recogn. 37 (1), 1–19.